CHAPTER IV

LIGHT INTENSITY ATTENUATION DEVICE: VARIABLE OPTICAL ATTENUATOR

4.1 INTRODUCTION

Variable Optical attenuators (VOA) with large attenuation range and high response time play an increasingly important role in fiber-optic networks. The main applications of VOA are in power tuning of lasers and detectors, in gain control and flattening of optical amplifiers and in optical device protection. Commercially available variable optical attenuators are mainly based on optomechanical principles. They have the characteristics of low insertion loss ($<1.5dB$), low crosstalk, wavelength uniformity, low wavelength dependent loss (WDL), and low polarization dependent loss (PDL). However, the drawbacks of the existing VOAs are large in size, low operating speed, high cost and uncertain reliability. Due to the advanced MEMS fabrication technologies, different types of MEMS VOAs [64-73] that can overcome the above-mentioned problems by integrating fabricated chips with single mode fiber.

In this chapter, a variable optical attenuator using the newly developed thermal actuator array with dual shutters is developed. First, the configuration of proposed variable optical attenuator included optical structure and thermal actuator arrays are introduced. The fabricated device using MEMS-SOI fabrication technology, which simplifies the traditional surface micromachining technology, is demonstrated in later section. Subsequently, the results of experiments are described in detail. Finally, a short conclusion is given.

4.2 The Configuration of Proposed Variable Optical Attenuator

4.2.1 Optical Structural Design

In the present study, the attenuator chip is designed to ease the fiber assembly process. Here, fiber alignment grooves with the size of 126 *um* width and 80 *um* depth are fabricated on the same SOI device wafer to increase final alignment efficiency. Moreover, dual shutters and fiber-end stopper are fabricated sufficiently small in order to bring fiber ends closer together. The two fibers are arranged horizontally and separated approxima tely 20 *um* in distance. According to theoretical calculation, the longitudinal offset effect produces the beam divergence loss. Here, the loss can be calculated using the following equations:

$$Z_R = \pi n W_G^2 / \lambda \tag{4-1}$$

$$\eta = \frac{1}{1 + (0.5 * Z_w / Z_R)^2} \tag{4-2}$$

where Rayleigh distance (Z_R) denotes the beam wave that is radiated from the fiber end into a homogeneous medium; n is the refractive index; W_G is the core diameter (5um); and *?* denotes the wavelength (1.55um); By using equation (1), The Rayleigh distance Z_R is equal to 50.6708 um. Since the longitudinal offset distance, Z_w is equals to 20um, from equation (2), the theoretical light loss due to the beam divergence is about 0.16dB ($\log_{10}\eta$).

The advantages of using dual shutters are: (1) decrease applied driving voltage; (2) produce nearly linear response in voltage vs. attenuation by altering

the total voltage (voltage sum between two thermal actuator arrays) vs. total displacement function [74]. In order to avoid back-reflection from the input light on the shutter and output fiber back into input fiber, the shutter as well as the fiber end face is aligned at an 82° angle with respect to fiber alignment groove and fiber end face is 8° angle polished with antireflective coating. In order to improve the poor PDL characteristic of shutter type VOAs, the shutter end face is designed in profiled blade with small angle. For the present VOA design, the device is required to possess large overall displacement and low driving voltage in order to produce large attenuation range. To drive the shutters into the optical path of the fiber, a newly developed thermal actuator array is used. The VOA design can be realized using MEMS technology as schematically shown in Fig. 4.1.

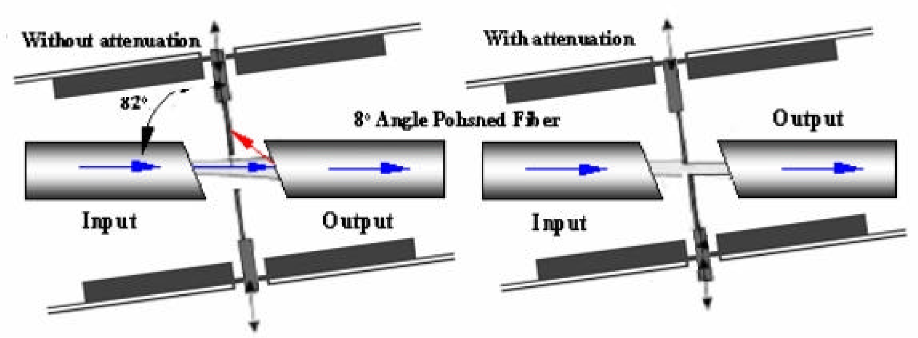

Fig. 4.1 Schematic of proposed optical variable attenuator with two-way shutters

4.2.2 THERMAL ACTUATOR DESIGN

Simple and effective actuators can be designed and manufactured using thermal effect in silicon [75, 76]. It is known that thermal actuators can produce larger displacement than electrostatic force with low applied voltages. A typical U-shaped lateral electro-thermal actuator generates deflections through

asymmetric heating of the narrower hot and wider cold beams. The higher current density in the narrower hot beam causes it to heat and expand more than the cold beams. The beams are joined at the free end which forces the actuator tip to move laterally. According to the principle, a horizontal pair thermal actuator combines tethers with a shutter that cancels out their arcing and expanding motion, producing a purely linear motion of the shutter.

The shape of tethers plays an important role in determining the motion efficiency of thermal actuator array. One of the presented thermal actuator array with 80um thickness comprise single crystal silicon is illustrated in Fig. 4.2. The main differences of the designed actuator arrays are in the tether shape, tether size and the connection location with actuators. In the present simulation, the dimensions of different type actuator array are shown in Table 4.1. The design is simulated by commercial software, CoventorWare. In order to compare with the different tether designs, the material properties of single crystal silicon are given as follow: Young's modulus E=170Gpa, Poisson ratio=0.25, Coefficient of thermal expansion CTE=2.5E-6, resistivity ρ =1E-2 Ω -cm. Here, the temperature-dependent parameters such as variation of thermal conductivity and specific heat are extracted from reference [77].

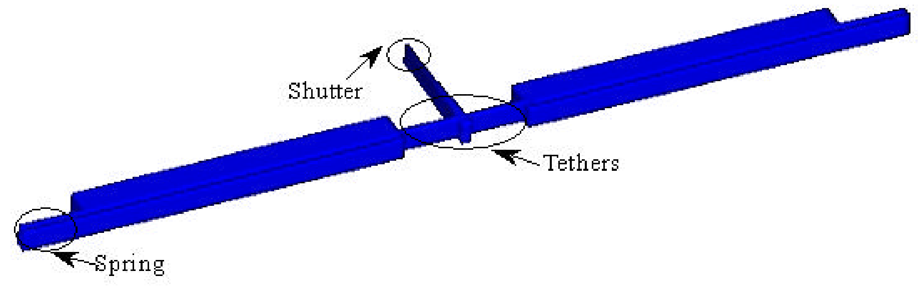

Fig4.2 The schematic drawing of cross type thermal actuator array

With these data, the displacement of the thermal actuator array affected by applied voltage can be simulated and the characteristics of the thermal actuator are obtained. The thermal actuator with different tether designs is also under investigation where the relationship of applied voltage vs. displacement and temperature are shown in Fig. 4.3 (a-b). By examining the simulation results, we note that the CS-type thermal actuator arrays produce the most efficient displacement than other designs [74]. All of the simulated maximum temperature is similar due to the fact that the resistance (~180Ω) is determined by hot beam. According to the simulation results, we concluded that for identical thermal actuator with different connected tether locations and tether shape play the major factors in affecting the displacement of the shutter.

Actuator name	SLH	LLH	SLC	CS_200um	CS_100um
Cold beam width	*100um*	*100um*	*100um*	*100um*	*100um*
Cold beam length	*995um*	*995um*	*995um*	*995um*	*995um*
Hot beam width	*10um*	*10um*	*10um*	*10um*	*10um*
Hot beam length	*1195um*	*1195um*	*1195um*	*1195um*	*1095um*
Spring width	*10um*	*10um*	*10um*	*10um*	*10um*
Spring length	*200um*	*200um*	*200um*	*200um*	*100um*

Tether width	15um	15um	15um	15um	15um
Tether length	103um	183um	103um	180um	180um
Tether type					

Table 4.1 The dimensions of five different VOA designs

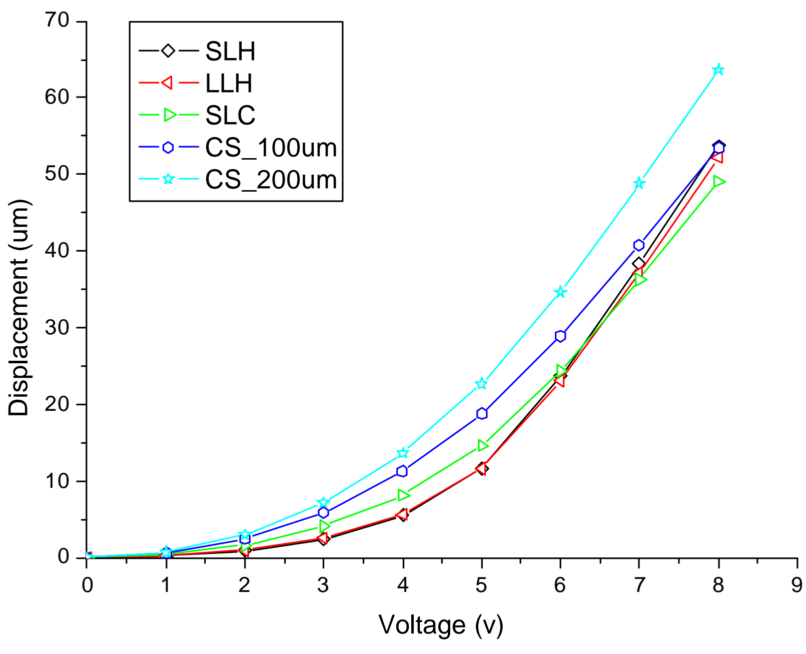

(a)

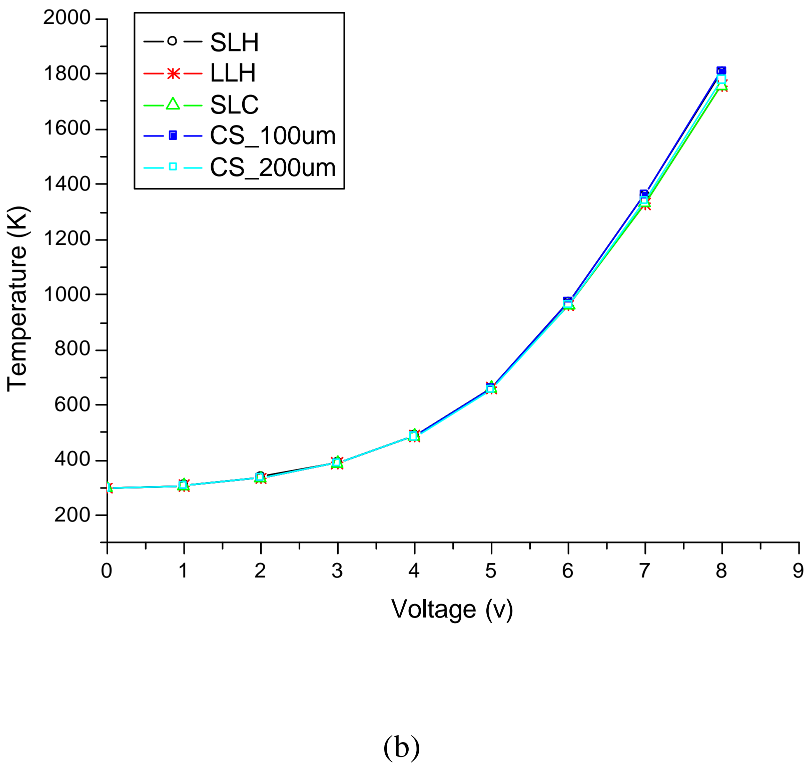

(b)

Fig4.3 (a-b) The simulation data of deflection and highest temperature vs. applied voltage for different thermal actuators

4.3 FABRICATION PROCESS

The advantage of using the silicon-on-insulator (SOI) technology is to greatly simplify the fabrication process of MEMS devices. However, in processing SOI wafer, the most critical step is the inductive coupling plasma (ICP) etching that determines the final outcome of the structure and the surface roughness of sidewall in fabricating designed optical devices.

The fabrication steps of the MEMS based VOA are shown in Fig. 4.4 (a-g). Here, the chosen SOI wafer for the fabrication process is a 500 *um* thickness substrate, 2 thickness buried oxide layer and 80 *um* thickness device wafer with 0.01Ω-cm resistivity (Fig. 4.4a). The reason that we choose 80 *um* thickness device wafer is to produce sufficient fiber alignment groove depth for future

embedded fiber. In the first step of the fabrication process, lift-off technology is used to deposit chromium and gold for the purpose of finishing connecting pads (Fig. 4.4b). This step avoids difficult photolithography process after deep silicon etching is performed. Secondly, we use the photolithography to pattern the designed thermal actuator and fiber alignment groove (Fig. 4.4c). The photoresist is then used to dry etch the device wafer by ICP (Fig. 4.4d). The buried oxide serves as an etching stop for ICP for the reason that etching rate is affected by the size of etching area. Note that etching rate will vary for different depth that affects the roughness on the sidewall. Once ICP etching is completed, resist is moved by acetone. To release the structures, the buried oxide has to be removed using BOE (Fig. 4.4e). Etching holes are opened to decrease etching time that is depending on undercutting effect. To avoid metal that is deposited on the top of the thermal actuator, which may produce bimorph effect, shadow mask technology is applied. Gold is deposited by sputter that increases the reflectivity of shutter (Fig. 4.4f). By integrating optical fiber in alignment grooves with thermal actuator, tether and shutter, we are able to assemble the final variable optical attenuator structure (Fig. 4.4g). Fig. 4.5(a-b) shows the SEM view of CS_type attenuator without/with optical fiber.

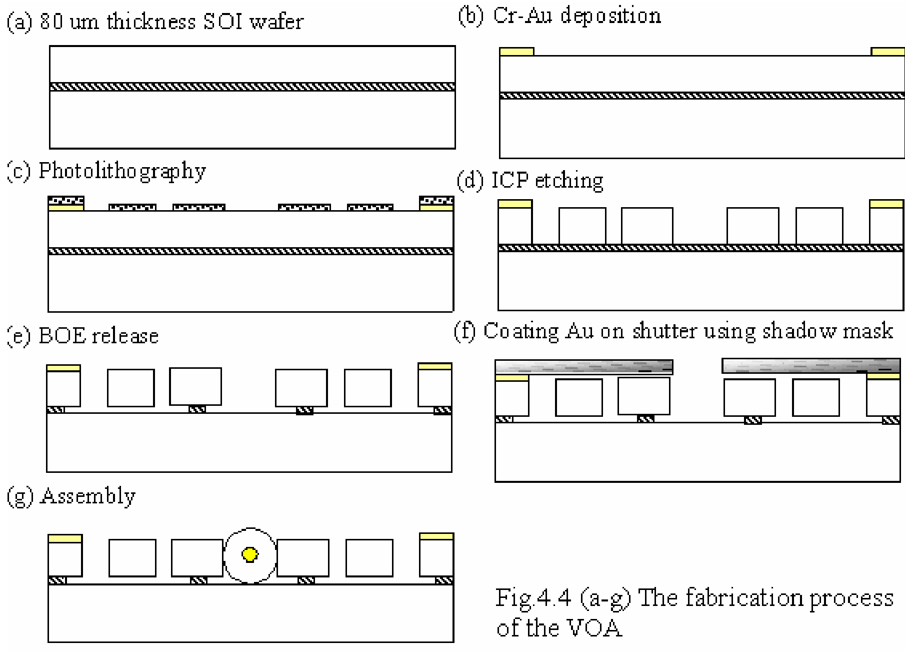

Fig.4.4 (a-g) The fabrication process of the VOA

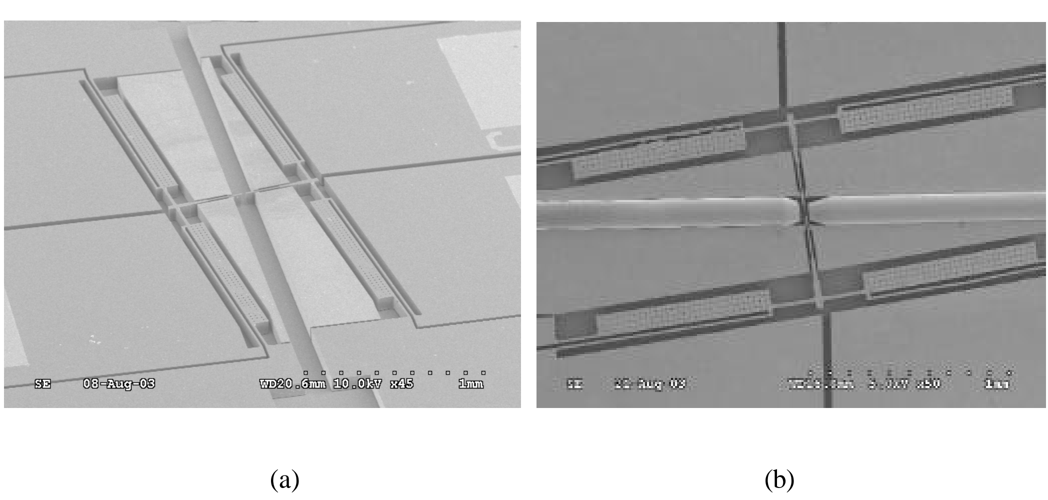

(a) (b)

Fig. 4.5 The SEM view of CS_type attenuator: (a) without optical fibers; (b) with optical fibers

4.4 EXPERIMENTAL RESULT

In order to characterize the designed VOA, a fiber alignment mechanism is used to integrate fibers on the fabricated MEMS chip. The equipment consisted of a 3D adjusting rod and rotation rod to adjust fiber misalignment. First, we insert the input fiber onto the mechanism. Note that, the size of the fiber diameter is 125

um and the tapered tip angle is 8°. By tuning the 3D adjusting rod, we are able to lead the fiber into the fiber alignment groove. Then, by tuning the rotation rod, the orientation of the fiber end face is adjusted until it is parallel to the shutter. UV-glue is injected into etched caves to fix input fiber. After inserted input fiber on the MEMS chip, same alignment procedure is used to insert output fiber with the help of power meter. Fig. 4.6(a-b) shows the final distance (41.4 *um*) between two inserted fibers once the assembly processes were completed. Here, the measured distance between two fibers is more than the designed distance. Theoretical light loss due to the beam divergence at this distance is 0.63*dB*. Other obstructing factors included the fiber misalignment and imperfect measurement conditions that produce loss at different wavelengths (1310 *nm* and 1550 *nm*) are due to that fact that we use the 1550 *nm* single mode fiber to measure 1310 *nm* light source. This may produce higher loss and dispersion in 1310 *nm*. The final measured insertion loss is 1.23*dB* and 1.54*dB* at 1550 *nm* and 1310 *nm* respectively. The initial return loss is 50*dB* and 56.8*dB* at 1550 *nm* and 1310 *nm* respectively.

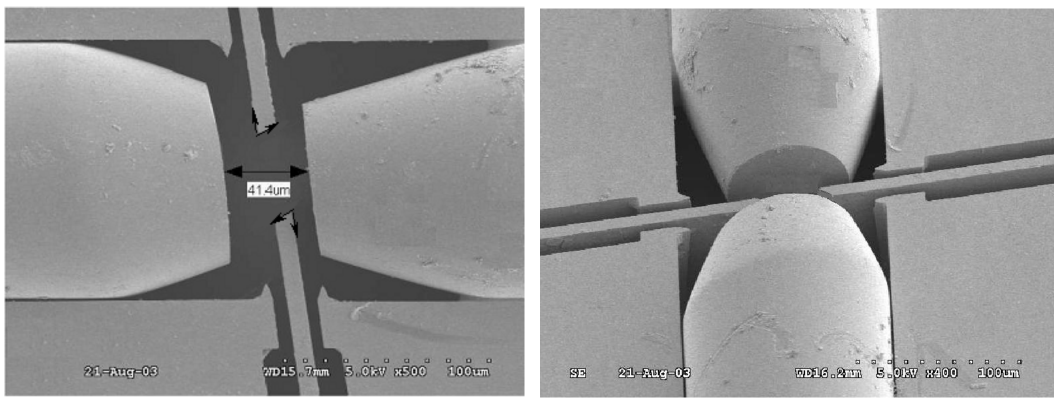

(a) Top view (b) Bird's eye view

Fig. 4.6 (a-b) The SEM views of fiber orientation after alignment

The static characteristic of the five thermal actuator arrays is shown in Fig. 4.7, which is measured by ***WYKO*** interferometer. Since the simulation and the measured data have similar tendency, thus, in Fig. 4.8, the static measured and simulation data of deflection and differential temperature vs. applied voltage for CS_200_type thermal actuators is given. The static temperature data is measured by ***QFI*** infrared scope. The errors between simulation and experiment are produced by the temperature dependent material properties, gas convection and radiation conductivity that are ignored in the simulations. According to the experiment results, the MEMS based VOA using thermal actuator array design can be driven under 5 V with working temperature under 550K. Note that, the low working temperature will increase the reliability of the thermal actuator arrays composed of single crystal silicon. Fig. 4.9 shows the fatigue test results of the thermal actuator array by operating the device 10^9 test cycles. It shows that by using single crystal silicon to manufacture driving component of VOA greatly enhanced the survivability of the device.

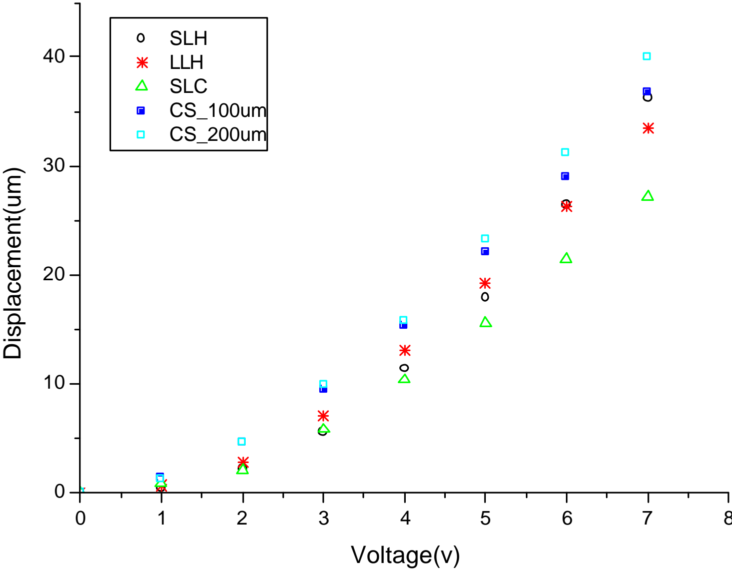

Fig. 4.7 The static measured data of deflections vs. applied voltages

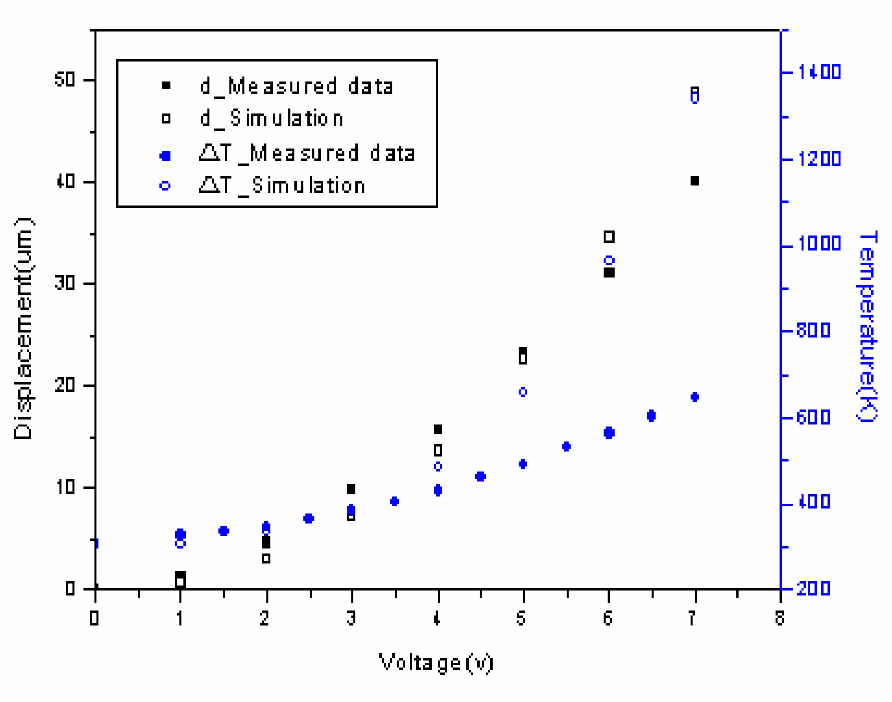

Fig. 4.8 The static measured and simulation data of deflection and differential temperatures vs. applied voltages for CS_200_type thermal actuators

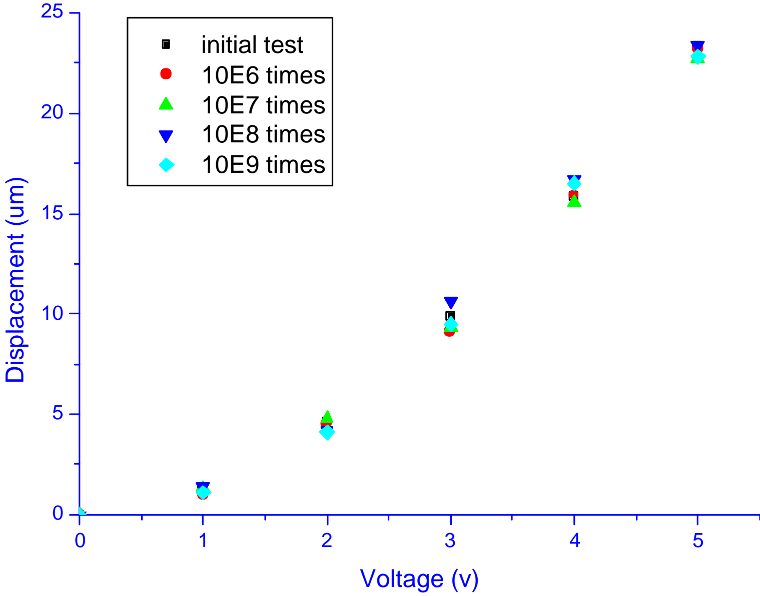

Fig. 4.9 the fatigue test results of the thermal actuator array through 10e9 test cycles

When the voltage on the thermal actuator is increased, the shutter is moved into optical path between the input and the output fiber, resulting in attenuation of the coupling. We have tried to improve tuning range and reduce operation voltages using two actuator arrays. The experimental results confirmed the present to actuator arrays indeed reduce the operation voltages to 3.5 V. However, as shown in Fig. 4.6(a), the profile defection of the shutters make the faced-to-faced wedge-shaped shutters can not isolated the incident light completely. Therefore the attenuation range can only achieved 28*dB*.

In the following experimental results, only one thermal actuator array is activated to attenuate the light intensity. Fig. 4.10 shows the schematic measurement structure of VOA. An ASE light source via input fiber through shutter transmits to output fiber. The output fiber connects with power meter that can be converted to electric signal read by oscilloscope. The relationship of attenuation and displacement vs. voltage is shown in Fig. 4.11. When applied voltage is over 2 V, the thermal actuator moves over 5um that actuated the shutter to come into the optical path of fibers. At 4.5V-applied voltages, the shutter covers the total optical path that obtains a maximum attenuation of 40*dB* and 46*dB* at 1550 *nm* and 1310 *nm* respectively. The Polarization Dependent Loss (PDL) is less 0.2*dB* at attenuation less 20*dB*. Unfortunately, as the attenuation is over 35*dB*, the PDL increases to 1.5*dB*. This drawback is produced by the diffraction effect at the poor shutter edge caused the higher PDL at higher attenuation range. The return loss at working situation is measured to be less than 45*dB*. The return loss is higher than initial return loss due to light scattering from the roughness of the shutter. Redesign the shutter shape and controlling the fabrication technique can improve the outcome of PDL.

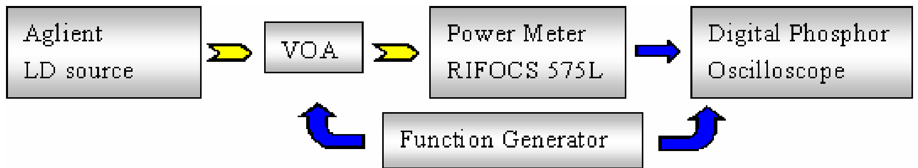

Fig. 4.10 The schematic measurement structure of VOA

The dynamic response of the attenuator is shown in Fig. 4.12. A square signal is applied to the VOA resulting in attenuation between 1.23*dB* to 40*dB*. The rise time and fall time of thermal actuator is 3.44 *ms* and 2.2 *ms* respectively. Note that, the phase shift of the test VOA is 1.2 *ms*. The response time of the thermal actuator array is compared with electrostatic comb drive fabricated by Marxer et al. which experienced 1 *ms* and 4.5 *ms* in rise time and fall time respectively [6]. The more comb-fingers the larger displacement can be obtained and in return we increase the actuator mass and decrease response time. Furthermore, to demonstrate the reliability of the device, a 3V square wave were used to drive the device about 100 cycles as shown is Fig. 4.13. The attenuation range changes from 15.787*dB* to 15.86*dB* and standard deviation is 0.019.

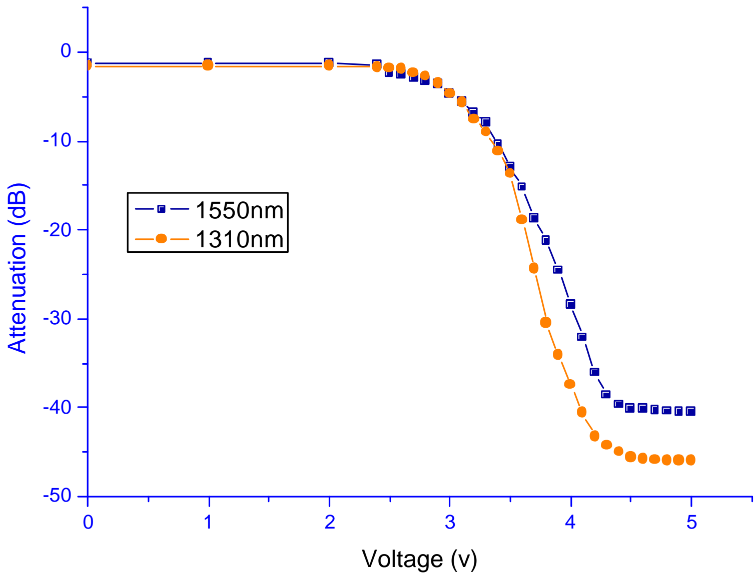

Fig. 4.11 The static attenuation vs. voltage characteristics of CS_200_type VOA

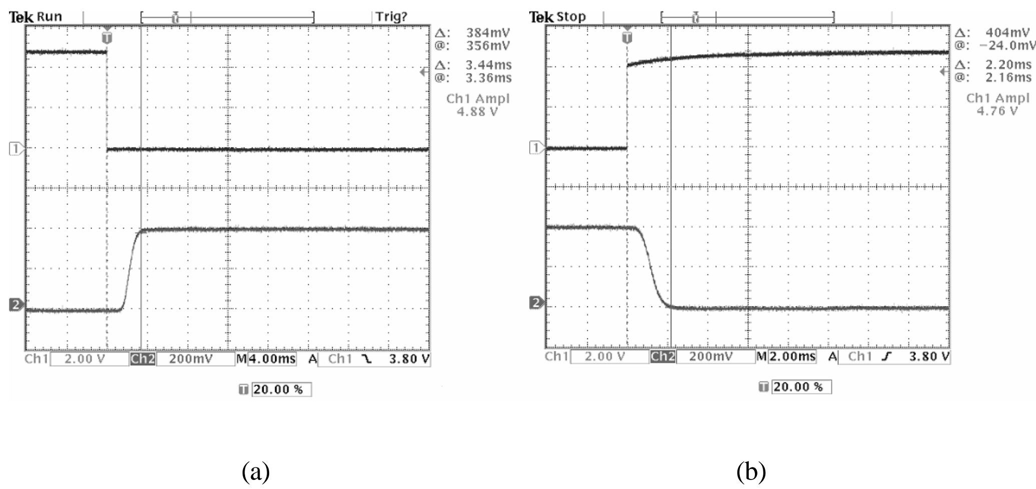

(a) (b)

Fig. 4.12 Dynamic response of CS_200_type VOA,(a) Switch OFF→ON：3.44ms (b) Switch ON →OFF：2.20ms

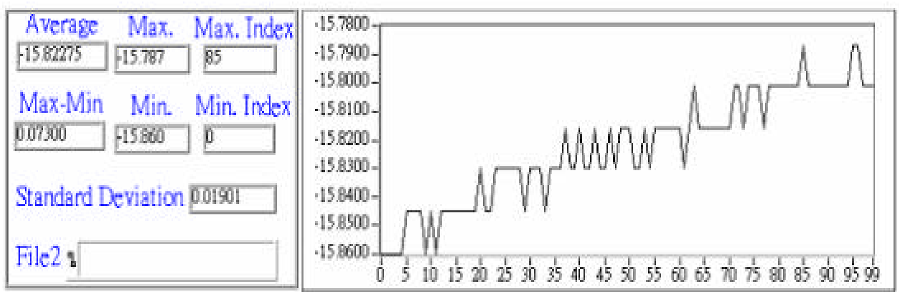

Fig. 4.13 The attenuation change through 100 cycles

4.5 SUMMARY

A compact optical variable attenuator (VOA) driving by thermal actuating principle with dual shutters for single mode fibers is developed in this chapter. The structure is fabricated through the SOI- MEMS technology processes. The present process greatly simplifies the traditional surface micromachining technology and increases its corresponding reliability. Five different thermal actuator arrays have been designed and measured. The newly designed thermal actuator array is capable of traveling 20 *um* distance with less than 5V applied

voltage for VOA application. The insertion loss of the fabricated VOA is below 1.5dB. The initial return loss and working return loss is about 50*dB* and 40*dB* respectively. Experimental results indicated that the response time is below 4 *ms* and maximum attenuation range is about 40 *dB* and 45*dB* at 1550 *nm* and 1310 *nm* respectively. The working voltage and temperature of the designed VOA is under 5V and 550K respectively. From experimental and simulation results, we concluded that the cross shape tether can produce the best displacement efficiency for VOAs application.

In the next chapter, dual directional vertical comb-drive actuator is introduced. The actuator can be used to develop moveable carriers with bi-direction motion which is suitable as tunable components for optical application. Moreover, a multi-layers SOI process with self-alignment is demonstrated to constuct the dual directional vertical comb-drive actuator.

CHAPTER V

LIGHT PATH SELECTION DEVICE: OPTICAL SWITCHES WITH DUAL COMB-DRIVE OPTICAL SWITCHES

5.1 INTRODUCTION

High-performance MEMS device can be fabricated and widely applied which heavily depend on the simplification of the fabrication steps to enhance the reliability and yields of fabricated MEMS devices. SOI-MEMS process has recently attracted increasingly interests as a main fabricating method to overcome the limitations of residual stress of deposited films and mirror area for optical MEMS applications [78-84]. Furthermore, optical devices such as scanning mirror devices may require large deflection angles or large actuation force characteristics with multi-directional/axis motion and good reliability [83,87]. For such application, single-crystal silicon microstructures and three-dimensional processes for fabrication of polysilicon microstructures have been previously demonstrated [78-88].

In the chapter, a novel method for fabricating a self-aligned electrostatics vertical comb drive using a multi-layer SOI process is developed. The actuating principle and simulation are illustrated. The comb fingers with self-aligned and patterned are completed in a successive etching process and simultaneously separate upper and lower electrodes without critical alignment. This not only greatly simplifies the fabrication process, but also provides a solution to create realistic dual comb-drive optical switches. At last, the experimental results and

conclusion are given.

5.2 ACTUATING PRINCIPLE AND SIMULATION

A dual comb-drive optical switch with a pair spring beam is shown schematically in Fig.5.1. The comb fingers consist of three structure layers including polysilicon, nitride and single crystal silicon.

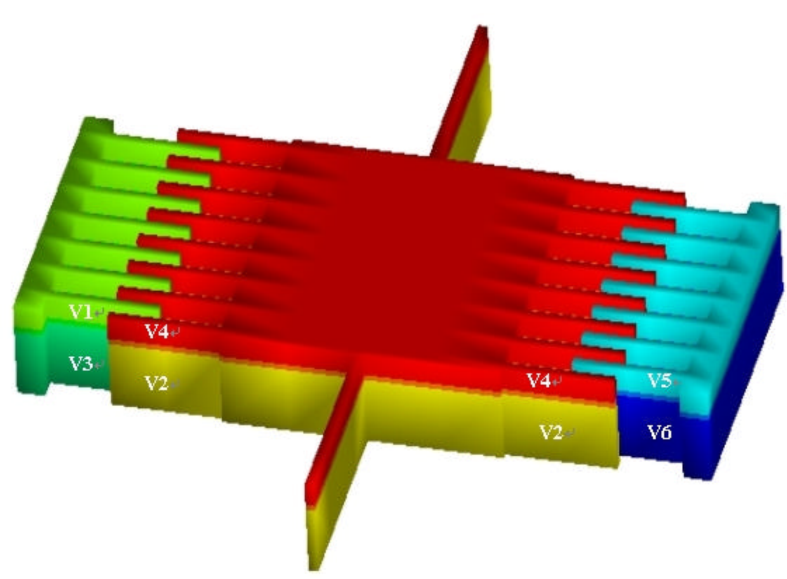

Fig.5.1 Schematic structure of dual comb-drive optical switches

The fixed and moving comb fingers are separated upper (*V1, V4, V5*) and lower (*V2, V3, V6*) electrodes by nitride layer. The electrodes of the dual comb-drive optical switches are divided into six individual contacting pads that are able to produce multi-directional motion. As shown in the Table 5.1, when voltage is applied between electrodes *V1*, *V2* and *V5*, the imbalance of the electric field distribution results in a vertical induced force. And consequently, moving comb fingers enable upward motion. On the other hand, when voltage is applied between electrodes *V3, V4* and *V6*, moving comb fingers enable downward motion. If we apply voltages between *V1, V3* and *V2, V4*, or *V5, V6* and *V2, V4*,

moving comb fingers produce horizontal motion like a lateral-axis comb drive [90]. Furthermore, by applying voltage between *V1, V2* or *V6, V4*, the structure with moving comb fingers can convert vertical force to clockwise rotation directly. On the contrary, by applying voltage between *V5, V2 or V3, V4* that could produce counterclockwise rotation. The simulation results are shown in Fig.5.2.

	Electrode	V1	V3	V5	V6	Motion
(a)	V2	+	−	+	−	↑
(b)	V4	−	+	−	+	↓
(c)	V2&V4	+	+	+	+	← →
(d)	V2&V4	+	−	−	+	↷
(e)	V2&V4	−	+	+	−	↶

Tab.5.1 Multi-directional motion principles: (a) upward motion; (b) downward motion; (c) horizontal motion; (d-e) rotational motion

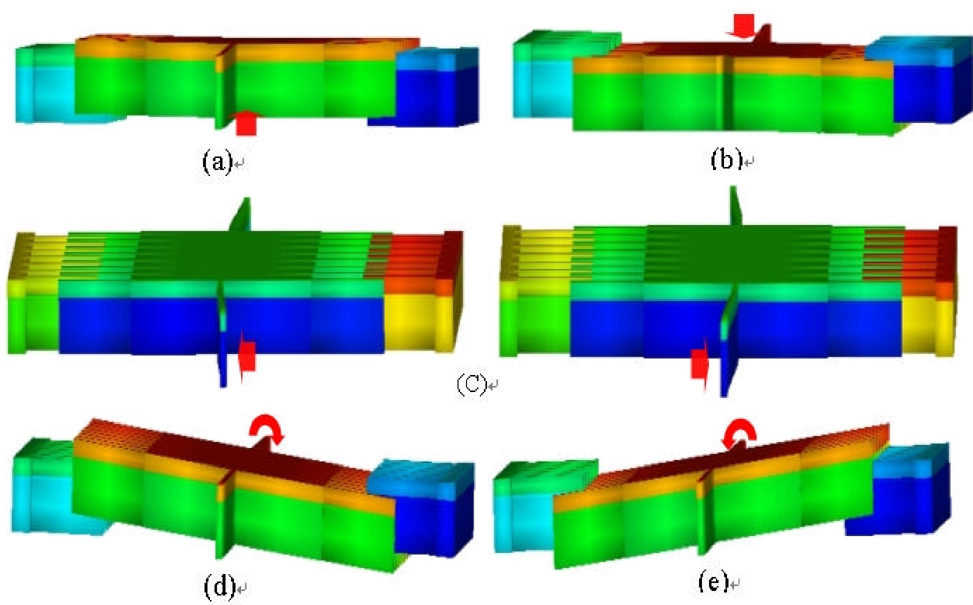

Fig.5.2 Simulation results of dual comb-drive optical switches: (a) upward motion (b) downward motion (c) horizontal motion (d-e) rotational motion

Note that, vertical comb-drive actuator with limited displacement is determined by the device layer thickness [89]. The larger thickness of the comb fingers, the more vertical displacement it will produce. In order to evaluate the relationship between voltage and displacement, force balance equation is needed in the present analysis. The electrostatic energy that is used to deflect the actuator is converted to mechanical potential energy. When a voltage is applied between the upper and lower electrodes, the electrostatic force F_e is given by [88, 90]:

$$F_e = \frac{NL}{2}\frac{\partial C}{\partial z}V^2 \qquad (5\text{-}1)$$

where N is the number of pairs of comb fingers, L is the overlapped length of fixed and moving comb fingers, C is the capacitance between the separated electrodes, z is the displacement along the actuation direction, and V is the applied voltage. By using the ***ANSOFT Maxwell® 2D field simulator***, the relationship of capacitance and displacement of the two sidewall capacitors, *C12* and *C34,* i.e. up-capacitor and low-capacitor can be evaluated respectively. According to this relationship, the gradient versus static vertical displacement can also be determined. In the present simulation, the thicknesses of upper and lower electrodes are 2 *um* and 15 *um* thickness with 3 *um* comb finger gap. Fig.5.3a and 5.3b are used to show the simulation results of the capacitance versus displacement and the gradient capacitance gradient versus displacement respectively. The maximum displacement is obtained by the intersections of two gradient curves with the z-displacement axis, which occur at –4.14 *um* and 4.14 *um*. For a given input voltage, the electrostatic energy (F_e) is equal the mechanical energy (F_m) stored in the device. The relationship between displacement and applied voltage can be obtained by solving the force balance equation:

$$F_e = F_m = kz \tag{5-2}$$

where k is the spring constant. The result is plotted in Fig.5.4 for vertical motion of the dual comb-drive optical switches with 272 pairs comb fingers. Furthermore, when driving voltage increases, different spring constants will still produce saturated displacements at –4.14 *um* to 4.14 *um*.

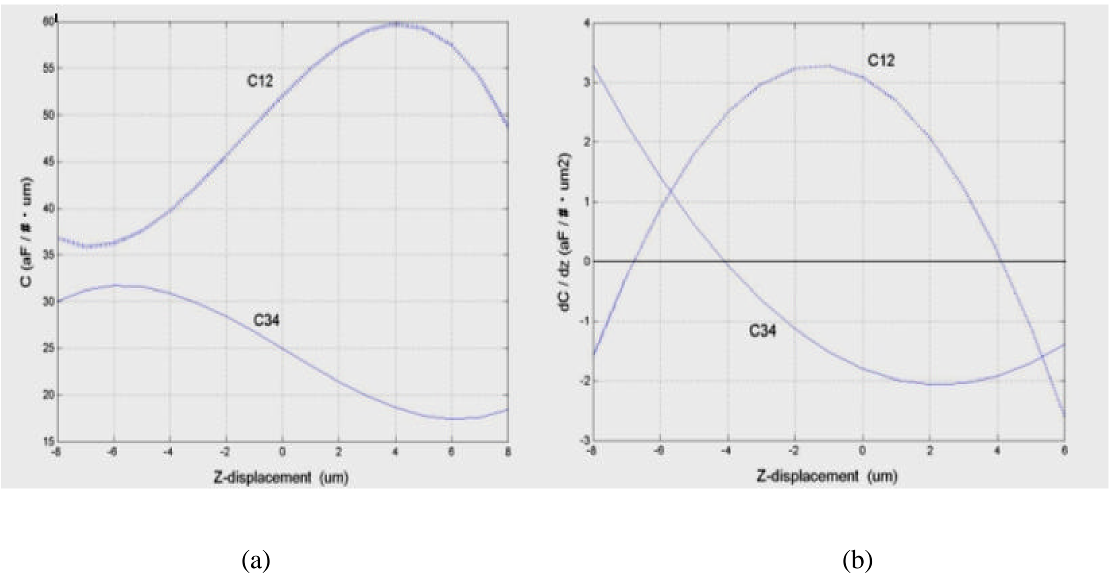

(a) (b)

Fig.5.3 Calculation results of vertical motion (a) capacitance vs. z-displacement (b) capacitance gradient vs. z-displacement

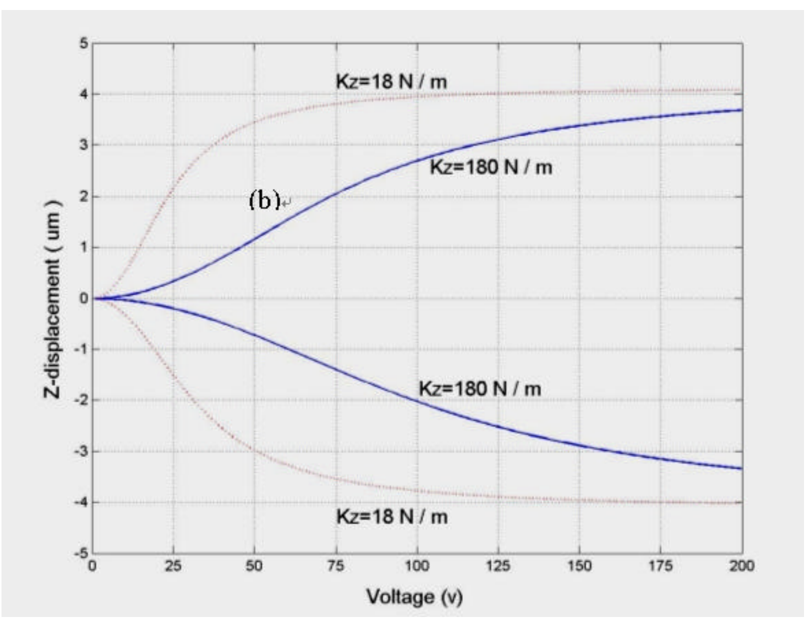

Fig.5.4 Calculation results of z-displacement vs. applied voltage

5.3 FABRICATION PROCESS

The present process based on SOI wafer consists of four photolithography masks: three front side etching masks for contact window, metal pads and ICP etching, and one backside etching mask to release the designed structures. The fabrication processes are schematically depicted in Fig.5.5. The present process used a high doping SOI wafer with 15 μm device layer (0.01~0.005Ω／□) , 3μm buried oxide and 450 *um* substrate. At first, a thin layer of thermal oxide (0.2um) and LPCVD nitride (0.5 *um*) are deposited on the wafer. In order to protect existed thermal oxide and nitride from front side etching, photoresist is spun on the backside wafer. Here, these deposited layers will be used as a mask for backside anisotropic etching. As illustrated in Fig. 5.5a, a 0.1 μm thickness of silicon nitride and a 2 μm thickness of high doping polysilicon are deposited on SOI wafer using LPCVD. The silicon nitride (200~400MPa) and polysilicon can be used as an insulation layer and structure layer. LPCVD polysilicon layer is deposited at 585±5℃ through POCL3 diffusion and 1050℃ 30 min. annealing that produces a residual stress less than 100MPa. A polysilicon sheet resistance less than 1Ω／□ was measured. Note that, the thickness of polysilicon can be changed depending upon the designed requirements. In other words, the LPCVD method can be replaced by an epitaxial method if thicker polysilicon is needed. Then, STS ICP and RIE are used to etch polysilicon and silicon nitride, respectively. The purpose of the above-mentioned etching steps is to create upper and lower contact-windows so that the electrodes on device layer and on the polysilicon can be patterned simultaneously (Fig. 5.5b). As shown in Fig. 5.5c, the Cr/Au layer is deposited and patterned on the device layer and the polysilicon to form connecting pads. In Fig. 3d, the device-nitride-polysilicon layer is patterned

and etched by interchanging STS ICP and RIE. By exchanging these processes, we are able to use one-mask-alignment to etch polysilicon, nitride and single crystal silicon, consecutively. Note that regardless of fixed or moving structures / upper or lower electrodes, the present step can be accomplished all in one mask. The advantage of the present step is to construct the fixed and moving structures with upper and lower electrodes with one mask. As illustrated in Fig. 5.5e, in order to etch LPCVD nitride and thermal oxide using RIE, the fourth mask is used on the backside of the wafer. Anisotropic etching is applied to etch silicon-substrate using KOH where etching stop will occur at the buried oxide. To avoid KOH attacking, a clamped apparatus is used to protect the front side silicon. Backside etching provides larger motion space for the device and decrease squeeze-film effect. In the final step, HF is used to etch the buried oxide below the comb fingers and structures (Fig. 5.5f). To prevent the side sticking of comb fingers produced in HF released step, CO_2 critical point dryer is used. Note that in the present self-aligned SOI process, the thickness of device-nitride-polysilicon layer can be changed depending on the characteristics of designed devices.

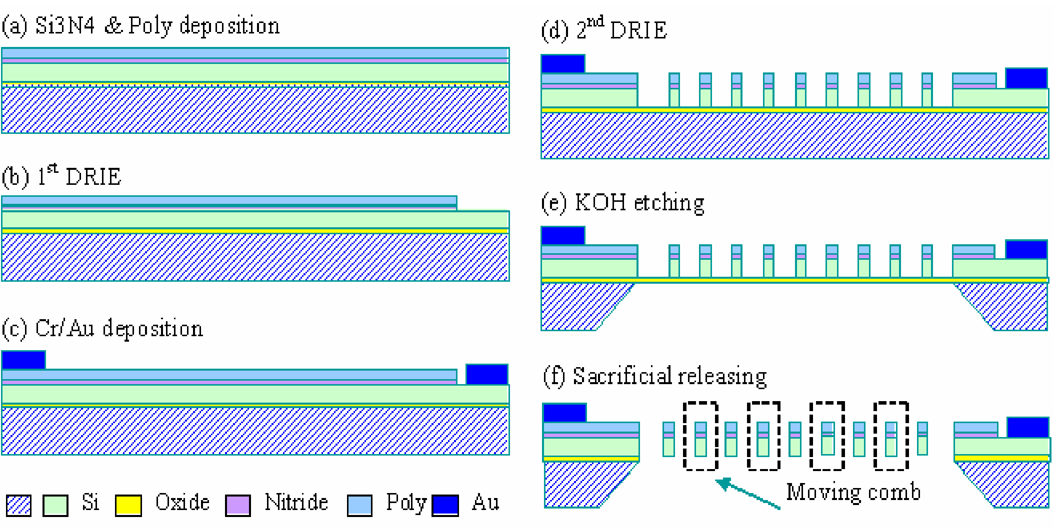

Fig.5.5 (a-f) Schematic fabrication processes flow

The proposed self-aligned multi-layers SOI process has been employed to fabricate the dual comb-drive optical switches, which is capable of creating piston motion. Figure 5.6 (a-b) show SEM pictures of the fabricated dual comb-drive optical switchess front side and backside. The large hole designed in the membrane is used to bond a DBR mirror. The dimensions of the designed device included a suspending membrane (1x1 mm^2), height 17 *um*, long 600 *um* and 10 *um*-wide springs, and 272 pairs of comb fingers (200 *um* long, 5 *um* wide) with 2 *um* gap. The oblique view of the comb fingers from bottom to top composite of single-crystal silicon; nitride and polysilicon that is shown in Fig. 5.7a and 5.7b. The measured dimensions of the fabricated device of each comb fingers width, air gap and spring width are 3.8 *um*, 3.2 *um* and 9.2 *um* respectively. The fabrication errors are due to photolithography inaccuracy and ICP undercut effects. The structure is constructed by single-crystal silicon with curvature at 5.7 meter. However upon a 0.2 *um* thickness gold film has deposited on the suspending structure, the curvature has decreased to 0.83 meter.

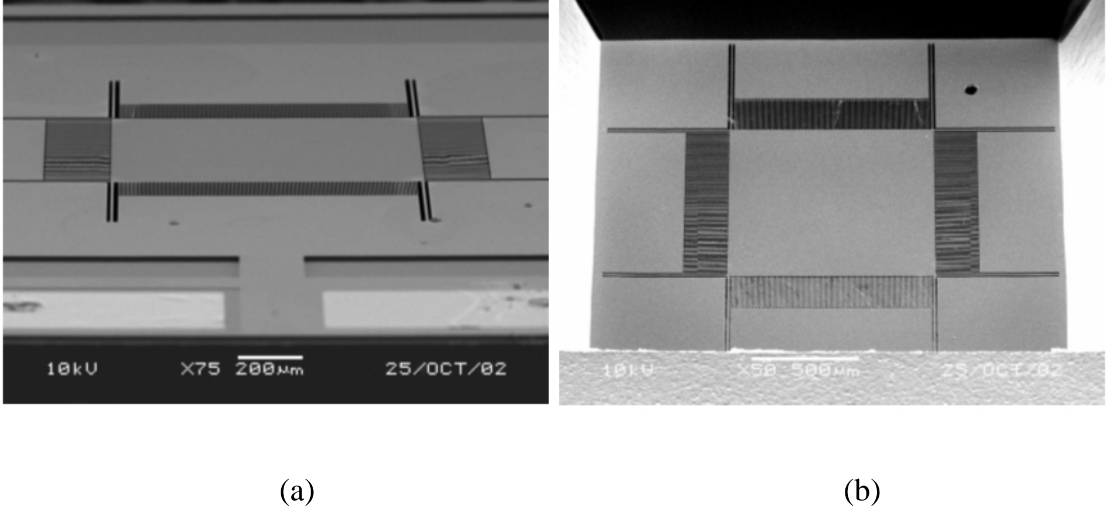

(a) (b)

Fig.5.6 The SEM pictures of dual comb-drive optical switches (a) front side (b) backside

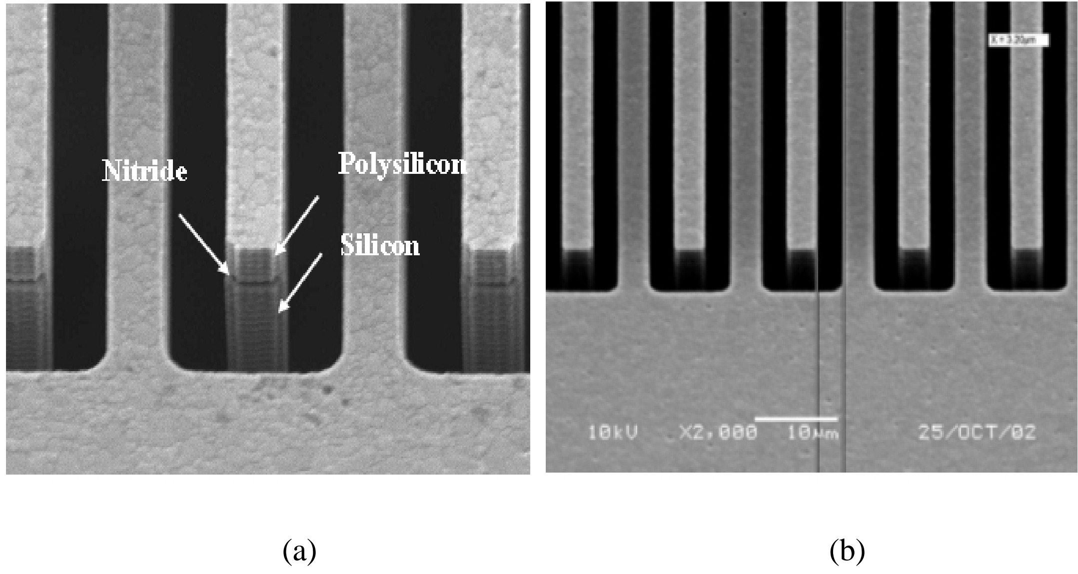

(a) (b)

Fig.5.7 The SEM pictures of fabricated comb fingers on the dual comb-drive optical switches

According to the fabrication method and operation principle, the dual comb drive structure incorporates a multi-directional motion microlens holder and a micromirror as shown in Fig. 5.8(a-b) and Fig. 5.9(a-b) respectively. Note that, the inner dual comb of the multi-directional motion microlen holder can move upward and downward while the outer dual comb can move horizontal. With the dual combs, the micromirror can move both clockwise and counterclockwise.

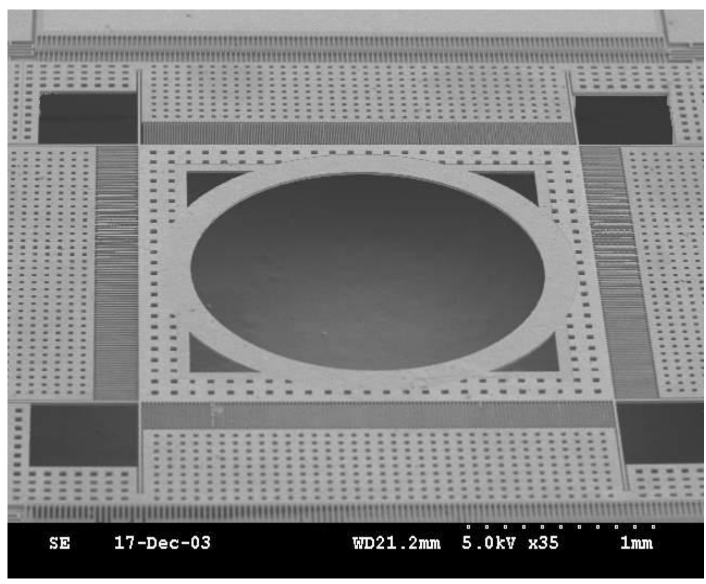

(a)

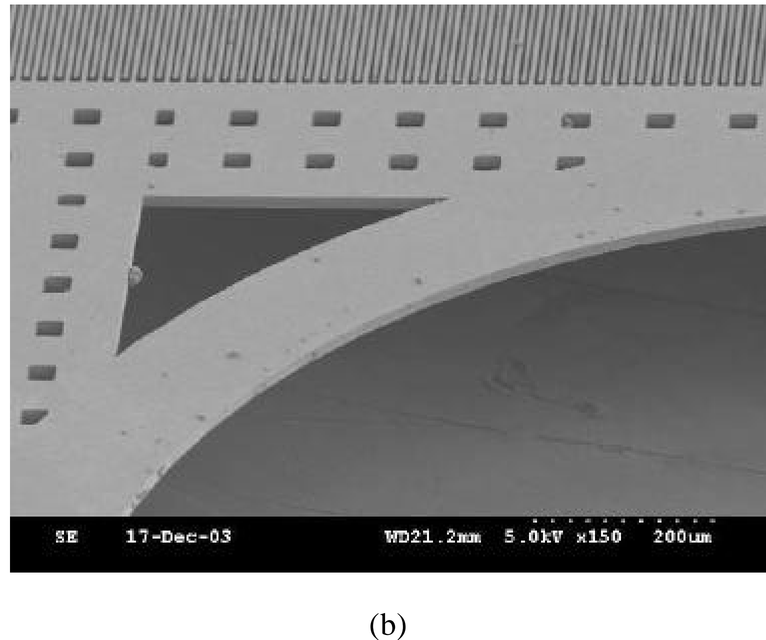

(b)

Fig.5.8 (a-b) The SEM image of a dual comb-drive optical switches with a microlen holder

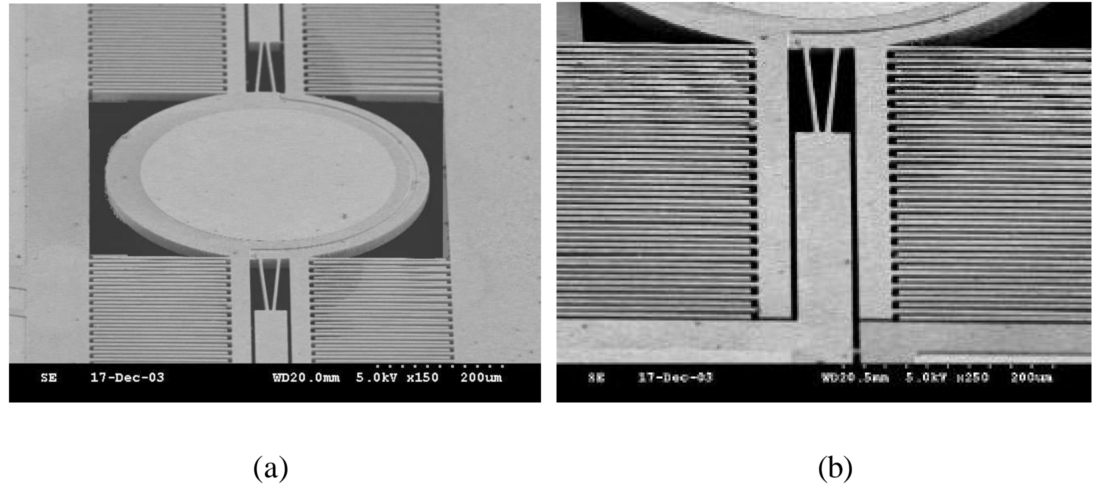

(a) (b)

Fig.5.9 (a-b) The SEM image of a torsion mirror with dual comb-drive structure

5.4 EXPERIMENTAL RESULT

The dimensions of the tested designed device included a suspending membrane (1x1 mm^2), height 17 *um*, long 750 *um* and 10 *um*-wide springs was designed and fabricated to actuate in z-axis direction. Eight spring beams that

eliminated x-y motions are used to support the suspending structure. As shown in Fig. 5.10, a Laser Doppler Vibrometer (LDV) is used to measure the dynamic characteristics of the dual comb-drive optical switchess. The first resonant frequency of the device is 5.46 kHz in vertical mode and the second resonant frequency is 21.86 kHz in the tilting mode. The corresponding simulations are carried out using *ANSYS*® simulation software where the resonant frequencies of vertical mode and tilting mode are 5.78 kHz and 23.3 kHz respectively. The spring constant of the fabricated devices is 180 Nt/m which is measured by nanoindentor. The dynamic displacement-voltage curve of the fabricated device is shown in Fig. 5.11. By using LDV, the actuator is capable of motion 6.87 u*m* downward and 9.53 u*m* upward with 80 V applied voltage in resonance frequency.

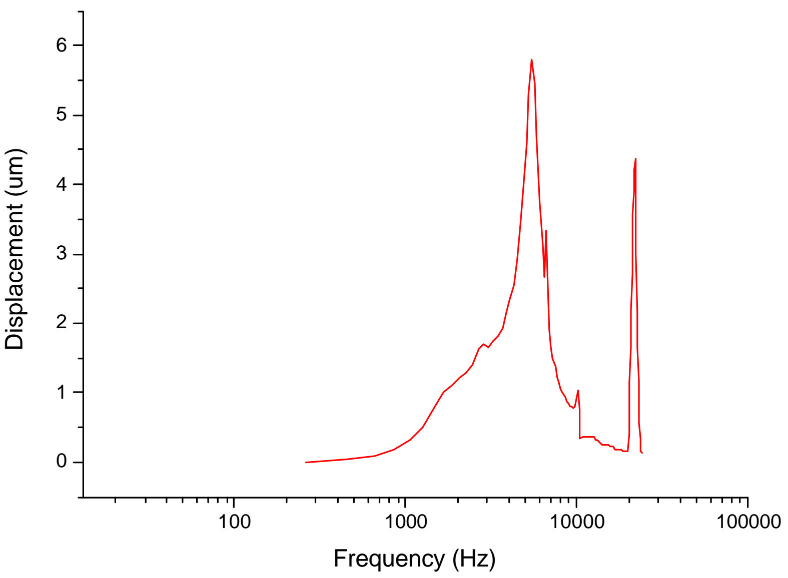

Fig.5.10 Resonant frequencies of the fabricated device

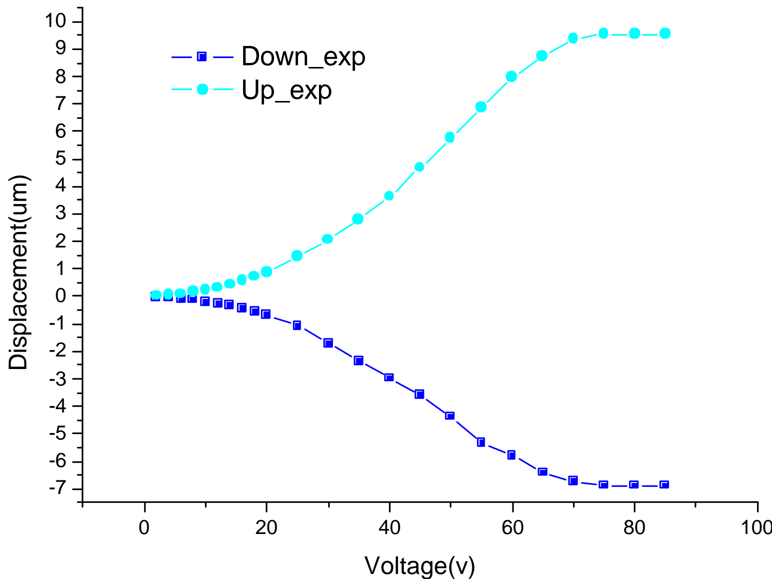

Fig.5.11 Z-displacement vs. applied voltages

Moreover, the torsional micromirrors using this technique have been fabricated as shown in Fig.5.9. The characteristic of the mirrors were accomplished using laser measurement equipments shown in Fig.5.12 Here, the incident light from laser is focused on the mirrors and reflected onto the screen. By applying different voltages and frequencies to actuate these devices, we could record the moving displacement of light spot on the screen such that the characteristics of tilt angle could be obtained. The resonant frequencies of the mirrors were measured by applying 60 *V* sine wave. The 1st and 2nd resonant frequencies of the torsional micromirror are at 16.76 kHz and 28.9 kHz respectively. The fig. 5.13 shows the voltage versus tile angle in the first resonant frequency. The results indicate that the micromirror could reach 35 +/- degree scan angles while applying 90 *V*.

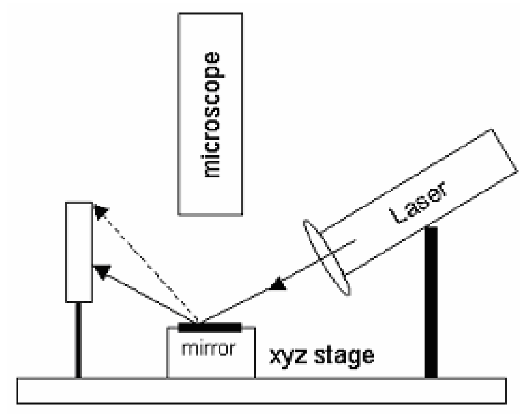

Fig.5.12 Schematic of laser measurement equipment

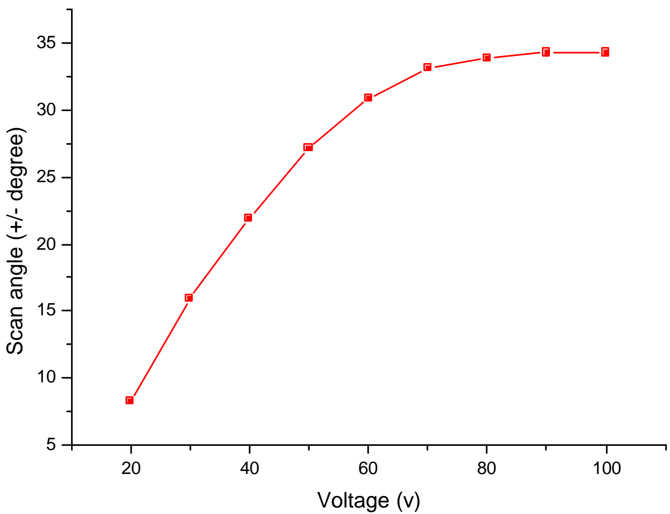

Fig.5.13 Scan angle vs. applied voltages in 16.76 *KHz*

5.5 SUMMARY

This chapter reports a novel method for fabricating a self-aligned electrostatics dual comb drive using multi-layers SOI process for MEMS applications. This technology provides several important features such as fixed or moving structures / upper or lower electrodes can be fabricated all in one mask that enhances yield and variety for high-performance MEMS devices. Furthermore, according to

design requirements, suitable SOI wafers like double bonding SOI wafers can be used to avoid existing complicated fabrication technologies. Using the proposed fabrication methodology and operation principle, we are able to manufacture various high-performance and various MEMS devices such as multi-directional motion microlens holder, Fabry-Perot filter, and scanning mirror.

CHAPTER VI

CONCLUSION

6.1 SUMMARY OF WORKS

The major contributions of this dissertation are to develop novel fabrication methods to fabricate MEMS devices for optical communication. In particular, low temperature surface micromaching and/or silicon-on-insulator technology are successfully used to fabricate tunable Fabry-Perot filter, variable optical attenuation and dual comb-drive optical switches. Commercial FEM simulation tools had been utilized to simulate the characteristics of the design devices.

First, a novel low temperature surface micromachining process (below 200℃) that is suitable for fabricating tunable Fabry-Perot filter is proposed. The advantages of the presented process consist of (1) materials used in this process are compatible with existing optical or IC process; (2) process and detected spectra are not limited by different substrates. Experimental results of the manufactured tunable Fabry-Perot filter indicated that the full width half maximum (FWHM) is closed to 1.3 *nm* and the measurement of reflectance of distributed Bragg reflectors is up to 99%. Note that within the 10 *nm* experimental tuning range, the FWHM is kept close to 1.3*nm* with tuning voltage from 0 to 30 voltages. The experimental results showed that the presented process has potential to apply to Wavelength Division Multiplexing (WDM) specifications of optical telecommunication. In particular, the process would also be integrated to fabricate tunable VCSEL processes.

Secondly, a compact optical variable attenuator (VOA) driving by thermal actuating principle with dual shutters for single mode fibers is developed. The fabricated thermal actuator array is capable of achieving larger displacement with low applied voltage than traditional thermal actuator array. The designed dual shutters can be driven independently or simultaneously, which increase the accurate tuning range and decrease working voltage for variable optical attenuator. The device is fabricated using MEMS-SOI fabrication technology, which greatly simplifies the traditional surface micromachining technology and increases its corresponding reliability. The newly designed thermal actuator array is capable of traveling 20 *um* distance with less than 5 *V* applied voltage for VOA application. The insertion loss of the fabricated VOA is below 1.5*dB*. The initial return loss and working return loss is about 50 *dB* and 40 dB respectively. Experimental results indicated that the response time is below 4 *ms* and maximum attenuation range is about 40 *dB* and 45 *dB* at 1550 *nm* and 1310 *nm* respectively.

At last, a novel method for fabricating a self-aligned electrostatics dual comb drive using a multi-layer SOI process is developed. The present method utilizes four aligned masks; wide greatly simplify the existing SOI-MEMS fabrication methods in manufacturing optical MEMS devices. Here, the actuating structure consists of fixed combs and moving combs that are composed of single crystal silicon, nitride and polysilicon. One mask is used to provide a deep etching to etch polysilicon, nitride and single crystal silicon respectively. The nitride separates polysilicon and single crystal silicon and provides an additional dielectric for the purpose of producing bi- directional motion upon applying electrostatic forces. A dual comb drive actuator with optical structures was fabricated based on the developed process. The actuator is capable of motion 250 *nm* downward and 480

nm upward with 30 *V* applied voltage. The dynamic characteristics of the first and the second resonant frequency of the dual comb-drive optical switches are 10.5 *kHz* and 23 *kHz* respectively. Moreover, the torsional micromirrors using this technique have been fabricated. The 1st and 2nd resonant frequencies of the torsional micromirror are at 16.76 kHz and 28.9 kHz respectively. The results indicate that the micromirror could reach 35 +/- degree scan angles while applying 90 *V*.

6.2 DIRECTIONS FOR FUTURE RESEARCH

In this thesis, the feasibility of the tunable Fabry-Perot filter, variable optical attenuator and dual comb-drive optical switches had been demonstrated preliminarily. The simplified fabrication methods had been developed to increase repeatability in manufacturing optical communication devices. The following suggestions are given for the future researches.

(1) Using the SOI-MEMS technology, the tunable Fabry-Perot filter that can improve the flatness of membrane and increase optical aperture. The characteristic of the tunable Fabry-Perot filter can be promoted. By varying the reflectance range of DBR, the tunable Fabry-Perot filter can be used not only in optical communication but also in biotechnology.

(2) Changing the arrangement of fibers and thermal actuators, we can form reflective-type VOAs to improve PDL loss.

(3) Integrating the control electronics with variable optical attenuator using SOI-MEMS technology, we able to develop compact, accurate VOA components for optical communication application.

(4) Increasing the thickness of upper and lower electrodes of dual comb-drive optical switch such that large displacement can be achieved for optical modulator, moveable lens holder and torsion mirrors.

REFERENCE

[1] Feynman, R. P., “Infinitesimal Machinery,” *IEEE J. Microelectromechanical Systems*, vol. 1, pp. 4-14, 1993

[2] Lober T.A., Howe R.T., “Surface-micromachining processes for electrostatic microactuator fabrication,” Solid-State Sensor and Actuator Workshop, 1988. Technical Digest., IEEE , , pp.59 - 62 6-9, June 1988

[3] ADI Introduces Industry’ s Smallest Accelerometers

[4] G.S. Chung, S. Kawahito, M. Ashiki, M. Ishida, and T. Nakamura, “Novel High-Performance Pressure Sensors Using Double SOI Structure,” *Tech. Digest, Transducers’91*, San Francisco, pp.676, 1991

[5] C. C. Beatty, “A Chronology of Thermal Ink-Jet Structures,” *Tech. Digest Solid-State Sensor and Actuator Workshop*, Hilton Head Island, SC, June 3-6, pp. 200-204, 1996.

[6] David W. Monk, and Richard O. Gale, “The Digital Micromirror Device for Projection Display,” *Microelectronic Engineering*, vol. 27, pp. 489-493, 1995.

[7] T. Li, “ The impact of optical amplifiers on long-distance lightwave telecommunications,” *Proc. IEEE 18*, pp.1568, 1993

[8] P. Trischitta, M. Colas, M. Green, G. Wuzniak, and J. Arena, “The TAT-12/13 cable network,” *IEEE Commun. Mag. 34*, pp. 24, 1996

[9] H. Taga, “Long-distance transmission experiments using the WDM technology,” *IEEE J. Lighrwave Technol. 14*, pp.1287, 1996

[10] M. C. Larson, and J. S. Harris, “Broadly-Tunable Resonant-Cavity Light-Emitting Diode,” *IEEE Photo. Tech. Lett*. 7 (11), pp. 1267-1269, 1995.

[11] Y. Uenishi, M. Tsugai, and M. Mehregany, “Micro-opto-mechanical devices fabricated by anisotropic etching of (110) silicon,” *J. of Micromech. Microeng.,* vol. 5, pp. 305-312. 1995.

[12] J. A. Walker, K. W. Goossen, and S. C. Arney, “Fabrication of a Mechanical Anti-Reflection Switch for Fiber-to-the-Home Applications,” *IEEE/ASME J. of Microelectromechanical Syst.*, vol. 5, no. 1, pp. 45-51, 1996.

[13] C. Marxer, M. A. Gretillat, N. F. De Rooij, R. Battig, O. Anthamatten, B. Valk, and P. Vogel, “Reflective duplexer based on silicon micromechanics for fiber-optic communication,” *IEEE J. of Light. Tech.*, vol. 17, pp115-122, 1999.

[14] D. E. Sene, V. M. Bright, J. H. Comtois, and J. W. Grantham, “Polysilicon micromechanical gratings for optical modulation,” *Sensors and Actuators A*, vol. 57, no. 2, pp. 145-151, 1996.

[15] S. S. Lee, L. S. Huang, C. J. Kim, and M. C. Wu, “Free-Space Fiber Optic Switches Based on MEMS Vertical Torsion Mirrors”, *IEEE J. of Light. Tech.*, vol. 17, no. 1, pp. 7-13, Jan. 1999.

[16] C. Marxer, and N. De Rooij, “Micro-Opto-Mechanical 2x2 Switch for Single Mode Fibers Based on Plasma-Etched Silicon Mirror and Electrostatic Actuation,” *IEEE J. of Light. Tech.*, vol. 17, pp. 2-6, 1999.

[17] Ford, J.E. ,and Walker, J.A.K., “Dynamic spectral power equalization using micro-opto-mechanics,” *IEEE photon. Tech. Letter*, vol. 107, pp. 1440-1442, 1998.

[18] Sang-Shin Lee, Yong-Sung Jin, Yung-Sung Son, and Tae-Kyung Yoo, “Polymeric tunable optical attenuator with an optical monitoring tap for WDM transmission network”, IEEE Photon. Technol. Lett., vol.11,no.5, May 1999.

[19] K.Bergman, N.Bonadeo, I.Brener, and K.Chiang, “Ultra-high capacity MEMS based optical cross-connects,” *Proc. SPIE*, vol.4408, Design, Test, Integration, and Packaging of MEMS/MOEMS 2001, Cannes, Frances, pp.2-5. 2001

[20] V.A.Aksyuk, D.J.Bishop; C.A.Bolle, R.C.Giles, F.Pardo,“Micro-electro-mechanical optical device,” US Patent 6,300,619, October 9, 2001.

[21] Tong, F.; Liu, K.; Li, C.-S.; Stevens, A.E.; Kwark, Y.H.,and Pezeshki, B.," A tunable receiver for packet-switched WDMA systems," *Lasers and Electro-Optics Society Annual Meeting, 1994. LEOS '94 Conference Proceedings. IEEE* , vol.1, pp.35 – 36,1994

[22] Tong, F.; Li, C.-S.,and Berkowitz, G.,"A 32-channel tunable receiver module for wavelength-division multiple-access networks,"Photonics *IEEE photon. Tech. Letter*, vol. 9, Issue. 11,pp.1523 - 1525 , Nov. 1997

[23] E. Bassous, " Fabrication of Novel Three-Dimensional Microstructures by the Anisotropic Etching of (100) and (110) Silicon," *IEEE Trans. Electron Devices*, vol.25, pp.1178,1978

[24] K.E. Petersen, "Silicon as a Mechanical Material," *Proc. IEEE*,vol.70, pp.420,1982

[25] R.D. Jolly and R.S. Muller," Miniature Cantilever Beams Fabricated by Anisotropic Etching of Silicon," *J. Electrochem. Soc.*, vol.127, pp. 2750,1980

[26] K.Petersen, "From Microsensors to Microinstruments," *Sensors and Actuators A*, vol.56, pp. 143,1996

[27] J.W. Gardner, *Microsensors: Principles and Applications*, Ch.3, John Wiley & Sons, 1994

[28] V. Milanovic, M. Last, and K.S. J. Pister, "Monolithic Silicon Micromirrors with Large Scanning Angle", *Optical MEMS' 01*, Okinawa, Japan, Sep. 2001.

[29] P. R. Patterson, D.Hah, H.Nguyen, H. Toshiyoshi, Ru-min Chao, and M.C. Wu, "A Scanning Micromirror with Angular Comb Drive Actuation", *IEEE International Conference on MEMS' 02*, Las Vegas, Nevada, USA, Jan.20-24, 2002

[30] D.B. Lee, "Anisotropic Etching of Silicon," *J. Applied physics*, vol.40, pp.4569,1969

[31] K.Beam, "Anisotropic Etching of Silicon," *IEEE Trans. Electron Devices*, vol.25, pp.1185, 1978

[32] E. Bassous," Fabrication of Novel Three-Dimensional Microstructures by the Anisotropic Etching of (100) and (110) silicon," *IEEE Trans. Electron Devices*, vol.25, pp. 1178, 1978

[33] J.A. Green and B.E. Burns, "Fabrication of Vertical Sidewalls by Anisotropic Etching of Silicon (100) Wafers," *J. Electrochem. Soc.*, vol. 141, pp.3182,1994

[34] H. Linde, C. Whiting and D. Benoit, "Etch Characteristics of Various Materials in Ethanolamine Etchants," *Sensors and Actuators A*, vol. 63, pp.251, 1997

[35] A. Merlos, M. Acero, M.H. Bao, J. Bausells and J. Estsve," TMAH/IPA Anisotropic Etching Characteristics," *Sensors and Actuators A*, vol. 37-38, pp.737, 1993

[36] M. J. Declercq, L. Gerzberg and J. D. Meindl," Optimization of the Hydrazine-Water Solution for Anisotropic Etching of Silicon in Integrated Circuit Technology," *J. Electrochem. Soc.*, vol. 112, pp.545,1975

[37] X. Li, M. Bao and S. Shen," Maskless Etching of Three-Dimensional Silicon Structures in KOH," *Sensors and Actuators A*, vol. 57, pp.47, 1996

[38] Nathanson, H. C., W. E. Newell, R. A. Wickstrom and J. R. Davis, "The Resonant Gate Transistor," *IEEE Trans Electron Dev.*, vol. 14, no. 3, pp.117-133, 1967

[39] Bryzek J., K. Petersen and W. McCulley, " Micromachines on the March," *IEEE Spectrum*, pp. 20-31, 1994

[40] C. H. Mastrangelo, and C. H. Hsu, "Mechanical Stability and Adhesion of Microstructures Under Capillary Forces – Part I: Basic Theory," *IEEE/ASME J. of Microelectromechanical Syst.*, vol. 2, pp. 33-43, 1993.

[41] http://www.memsrus.com/

[42] D. Koester, R. Mahedevan, B. Hardy and K. Marcus, "MUMPs Design Handbook," rev. 7, http://www.memsrus.com/, 2001.

[43] V. Milanovic, M. Last, and K.S. J. Pister," Laterally Actuated Torsional Micromirrors for Large Static Deflection" *IEEE Photonics tech. letters*, vol. 15, no. 2, 2003

[44] http://www.stsystems.com/

[45] Lawes, R.A.," Laser and electron beam based LIGA processes," *Microengineering - the Future!* , IEE Colloquium on13 Oct 1993, pp.7/1 - 7/3

[46] Patents DE4241045, US 5501893 and EP 625285, authors Franz Lärmer, Andrea Schilp

[47] Gwo-Bin Lee, Che-Hsin Lin and Guan-Liang Chang, " Multi-cell-line micro flow cytometers with buried SU-8/SOG optical waveguides," *The Fifteenth IEEE International Conference on Micro Electro Mechanical Systems*, pp.503-506, 20-24 Jan. 2002

[48] Houlet, L., Helin, P., Bourouina, T., Reyne, G., Diffour-Gergam, E., Fujita, H.," Movable vertical mirror arrays for optical microswitch matrixes and their electromagnetic actuation," *IEEE J. Selected Topics in Quantum Electronics*, vol. 8, Issue: 1, pp. 58 – 63, Jan.-Feb. 2002

[49] Farrokh Ayazi, and Khalil Najafi, "High Aspect-Ratio Combined Poly and Single-Crystal Silicon (HARPSS) MEMS technology," *J. Micromechanical systems*, vol.9, no. 3, pp. 288-294, 2000

[50] Lie, H.W., Dybvik, P.E. and Rygh, J., "SCREAM: screen-based navigation in voice messages, ", *Proceedings 1993 IEEE Symposium on Visual Languages*, pp.401-405, 24-27 Aug. 1993

[51] Huikai Xie and Gary K. Fedder, "Vertical Comb-Finger Capacitive Actuation and Sensing for CMOS-MEMS," *Sensors and Actuators A 95*, pp.212-221, 2002

[52] Riza, N.A., Polla, D.L., Robbins, W.P. and Glumac, D.E., "High resolution 50 nm linear displacement macroscale meander-line PZT actuator "*Electronics Letters*, vol. 29, Issue: 18, pp. 1606-1608, 2 Sept. 1993

[53] N. F. Raley, D.R.Ciarlo, J.C.Koo, B. Beiriger, J. Trujillo, C. Yu, G..Loomis and R. Chow, "A Fabry-Perot Micro-interferometer for visible wavelengths," *Solid-State Sensor and Actuator Workshop*, 1992. 5th Technical Digest, IEEE, pp.170-173

[54] J. Peerlings, A. Dehe, A. Vogt, M.Tilsch, C. Hebeler, F.Langenhan, P.Meissner, "Long Resonator Micromachined Tunable GaAs-AlAs Fabry-Perot filters," *IEEE Photonics Technology Letter*, Vol.9 , No.9, pp.1235-1237,1997

[55] P. Tayebati, P. Wang, M. Azimi, L. Maflah and D.Vakhshoori, "Microelectromechanical tunable filter with stable half symmetric cavity," *Electron. Lett.* , Vol.34, No.20, pp.1967-1968, 1998

[56] A.T.T.D. Tran, Y.H Lo, Z. H. Zhu, D. Haronian, and E. Mozdy, "Surface micromachined Fabry-Perot tunable filter," *IEEE photon. Technology Letter* Vol.8, no.3, p.393-395, 1996.

[57] E.C. Vail, M.S. Wu, G.S. Li, L. Eng and C.J. Chang-Hasnain, "GaAs micromachined widely tunable Fabry-Perot filters," *Electronics Letter*, Vol .31, No.3,pp. 228-229, 1995

[58] A.Spisser, R.Ledantec, C. Seassal, J. L. Leclercq, T. Benyattou, D. Rondi, R Blondeau, G. Guillot and P. Viktorovitch, "Highly Selective and Widely Tunable 1.55-um InP/Air-Gap Micromachined Fabry-Perot Filter for Optical Communications," *IEEE Photonics Technology Letter*, Vol.10, No.9, pp.1259-1261,1998

[59] M. Strassner , J. Daleiden, N. Chitica, D.Keiper, B. Stalnacke, S. Greek and K. Hjort ,"Ⅲ－Ⅴ semiconductor material for tunable Fabry-Perot filter for coarse and WDM systems," *Sensors and Actuators 85*, PP.249-255,2000.

[60] J. M. Vaughan, "The Fabry-Perot interferometer: history, theory, practice and applications, " Adam Hilger, 1989

[61] Eugene Hecht, "Optics" third edition, Addison Wesley, PP.409-418

[62] M.Born, E. Wolf, "Principles of Optics," 6th edition, Cambridge Press, reissued 1997

[63] H. A. Macleod, Thin-film optical filters, Adam Hilger Ltd, 2nd edition, 1986

[64] Sang-Shin Lee, Yong-Sung Jin, Yung-Sung Son, and Tae-Kyung Yoo, "Polymeric tunable optical attenuator with an optical mo nitoring tap for WDM transmission network," *IEEE Photon. Technol. Lett.*, vol.11,no.5, May 1999.

[65] Andersen B.M., Fairchild, S., Thorsten, N., and Aksyuk, V.," Mems variable optical attenuator for DWDM optical amplifiers," *Optical Fiber Communication Conference 2000*, vol.2 , pp.260 –262, March 2000

[66] N. A. Riza, "Fault-tolerant fiber-optical beam control modules," Patent No. 6,222,954, April 24, 2001.

[67] S. Sumriddetchkajorn and N. A. Riza, "Fault-tolerant three-port fiber-optic attenuator using small tilt micromirror device," *Optics Communications*, 205, 15 April 2002, pp. 77-86.

[68] Joseph E. Ford, James A. Walker, Dennis S. Greywall, and Keith W. Goossen, "Micromechanical fiber-optic attenuator with 3 us response," *J. of lightwave technol.*, vol.16, no.9, pp. 1663-1670, Sept. 1998.

[69] Cornel Marxer, Patrick Griss, and Nicolaas F. de Rooij, "A variable optical attenuator based on silicon micromechanics", I*EEE Photon. Technol. Lett.*, vol.11, no.2, pp.233-235, Feb.1999.

[70] Che-Heung Kim, Namkyoo Park and Yong-Kweon Kim," MEMS reflective type variable optical attenuator using off-axis misalignment," *Optical MEMS, IEEE/LEOS International Conference*, pp.55-56, Aug. 2002

[71] Tae-Sun Lim, Chang-Hyeon Ji, Chang-Hoon Oh, Youngjoo Yee, and Jong Uk Bu," Electrostatic MEMS variable optical attenuator with folded micromirror", *Optical MEMS, IEEE/LEOS International Conference*, pp.143-144, 2003

[72] Robert Wood, Vijay Dhuler, and Ed Hill, "A MEMS variable optical attenuator", *Optical MEMS, IEEE/LEOS International Conference*, pp.121-122, Aug. 2000

[73] Vijayakumar R. Dhuuler, Edward A. Hill, Ramaswamy Mahadevan, Mark David Walters, and Robert L. Wood," MEMS variable optical attenuator", patent No. US 6275320

[74] R.Wayne, Fuchs, and Barrie Keyworth," Micro-electro mechanical based optical attenuator", Pub. No.: US2002/0076191

[75] John H. Comtois, and Victor M. Bright, "Application for surface-micromachined polysilicon thermal actuators and arrays", *Sensors and Actuators A58*, pp.19-25, 1997

[76] Martin Hoffmann, Peter Kopka, and Edgar Voges, "Bistable micromechanical fiber-optics switches on silicon with thermal actuators", *Sensors and Actuators A78*, pp.28-35, 1999

[77] Aaron A. Geisberger, Niladri Sarkar, Matthew Ellis, and George D. Skidmore, "Electrothermal properties and modeling of polysilicon microthermal actuators", *J. of Microelectromechanical systems*, vol. 12, no.4, August 2003

[78] R. A. Comant, J. T. Nee, K. Y. Lau, and R.S. Muller, "A Flat High-Frequency Scanning Micromirror", Proc. Solid-State Sensor and Actuator Workshop, Hilton Head, U.S.A., pp.6-9, Jun 4-8, 2000.

[79] H. Schenk, Peter Durr, T. Haase, D. Kunze, U. Sobe, H.Lakner and Heinz Kuck, "Large Deflection Micromechanical Scanning Mirrors for Linear Scans and Pattern generation", IEEE J. of Selected Topics in Quantum Electronics, Vol. 6 No. 5, Sep./Oct. 2000

[80] V. Milanovic, M. Last, and K.S. J. Pister, "Monolithic Silicon Micromirrors with Large Scanning Angle", Optical MEMS' 01, Okinawa, Japan, Sep. 2001.

[81] U. Krishnamoorthy, and O. Solgaard, "Self-Aligned Vertical Combdrive Actuators for Optical Scanning Micromirrors", Optical MEMS' 01, Okinawa, Japan, Sep. 2001.

[82] S. Kwon, V. Milanovic, and L.P. Lee, "Vertical Microlens Scanner for 3D Imaging", Proc. Solid-State Sensor and Actuator Workshop, Hilton Head, U.S.A., pp.227-230, Jun 2-6, 2002

[83] P. R. Patterson, D.Hah, H.Nguyen, H. Toshiyoshi, Ru-min Chao, and M.C. Wu, "A Scanning Micromirror with Angular Comb Drive Actuation", IEEE International Conference on MEMS' 02, Las Vegas, , USA, Jan.20-24, 2002

[84] V. Milanovic, M. Last, and K.S. J. Pister, "Laterally Actuated Torsional Micromirrors for Large Static Deflection", IEEE Photonics Tech., Vol. 15, No. 2, Feb.2003.

[85] J.H. Lee, Y.C. Ko, D.H. Kong, J. M. Kim, K.B. Lee, and D.Y. Jeon, "Fabrication of Silicon Optical Scanner for Laser Display", 2000 IEEE/LEOS International Conference on Optical MEMS, Kauai, USA, pp.13-14, Aug. 21-24, 2000.

[86] K.A. Shaw, Z.L. Zhang, and N.C. MacDonald, "SCREAM I: A single mask, single-crystal silicon, reactive ion etching process for microelectromechanical structures," Sens. Actuators A, Phys., vol.40, pp.63-70, 1994

[87] U. Krishnamoorthy, K. Li, K. Yu, and D. Lee, "Dual-Mode Micromirrors for Optical Phased Array Applications", Transducer' 01, Munich, Germany, Jun.2001.

[88] A.Selvakumar, K.Najafi, W.H.Juan, S.Pang, "Vertical Comb Array Microactuators", 1995, Micro Electro Mechanical Systems, MEMS '95, Proceedings. IEEE,pp. 43-48

[89] J.-L. Andrew Yeh, C.Y. Hui and N.C. Tien, "Electrostatic Model for an Asymmetric Combdrive", IEEE J. Microelectromechanical System, Vol. 9, No. 1, March 2000.

[90] H. Xie, and G. K. Fedder, "Vertical Comb-Finger Capacitive Actuation and Sensing for CMOS-MEMS", Sensors and Actuators A95, pp.212-22

BIOGRAPHY

學歷

博士	國立交通大學 電機與控制工程學系	1999.9 ~ 2004.6
碩士	國立交通大學 電子物理學系	1996.9 ~ 1999.7
學士	國立交通大學 電子物理學系	1992.9 ~ 1996.7
高中	台北市立建國高級中學	1989.9 ~ 1992.7

經歷

助理工程師

全磊微機電	1998.8 ~ 1999.6
環國科技	1999.11~ 2001.2
慧亞科技	2000.7 ~ 2001.3

研究助理

國立交通大學 電機與控制工程學系	1999.1 ~
行政院國科會 精密儀器發展中心	2000.6 ~ 2001.12
經濟部微光電系統晶片研發計畫	2002.11

PUBLICATION

Journal paper

[1] **W. T. Lin**, J. C. Chiou and Bruce C. S. Chou, “A photonic device compatible process in fabricating tunable Fbary-Perot filter”, *Optics Communications 210,* pp.149-154, 2002

[2] Y. C. Lin, J. C. Chiou, **W. T. Lin**, Y. J. Lin and S. D. Wu, “The Design and Assembly of Surface-Micromachined Optical Switch for Optical Add/Drop Multiplexer Application”, *IEEE Transaction on Advanced Packaging,* vol. 26, no. 3, pp.261-267, 2003

[3] J. C. Chiou and **W. T. Lin**, “Variable optical attenuator using a thermal actuator array with dual shutters”, *Optics Communications* (Accepted)

[4] **W. T. Lin** , J. C. Chiou and Chingfu Tsou, “A Self-Aligned Fabrication Method of Dual Comb Drive using Multi-Layers SOI Process for Optical MEMS Applications”, *Microsystem Technologies* (Accepted)

Conference Paper

[1] Bruce C. S. Chou, **W. T. Lin** and J. C. Chiou, “Study of micromachined tunable filter and its potential application to tunable laser”, The 4th CLEO/Pacific Rim 2001, pp.418

[2] **W. T. Lin**, Bruce C. S. Chou and J. C. Chiou, “An novel low temperature process in fabricating tunable Fabry-Perot filter”, The Conference of 2001 IEEE/LEOS Optical MEMS, 2001, pp.71

[3] **W. T. Lin** and J. C. Chiou,, “Multi-directional dual comb-drive actuator for optical applications”, The International Conference on Materials for Advanced Technologies

Patent

[1] **周正三、邱俊誠、林煒挺…等六人，”電容式壓力為感測元件及其製造方法與訊號讀取方式”。中華民國專利** 541503 **號，民國** 92 **年。**

Other

[1] **林煒挺、周正三、邱俊誠，”微型光學調頻元件及其應用趨勢”，光訊，第九十四期，**pp.7-10，2002。